CHINESE OPTICS LETTERS

Vol. 22, No. 4 | April 2024

Eye-safe intra-cavity diamond cascaded Raman laser with high peak-power and narrow linewidth

Xiaobo Mi (米晓波)[1,†], Chaonan Lin (林超男)[1,†], Yongsheng Hu (胡永生)[1*], Houjie Ma (马后杰)[1], Jiuru He (何九如)[1], Fengying Ma (马凤英)[1], Li Fan (樊 莉)[2**], and Chongxin Shan (单崇新)[1***]

[1] School of Physics and Microelectronics, Zhengzhou University, Zhengzhou 450001, China

[2] College of Physics Science and Technology, Institute of Applied Photonic Technology, Yangzhou University, Yangzhou 225002, China

[†]These authors contributed equally to this work.

*Corresponding author: huyongsheng@zzu.edu.cn

**Corresponding author: fanli@yzu.edu.cn

***Corresponding author: cxshan@zzu.edu.cn

Received October 7, 2023 | Accepted December 11, 2023 | Posted Online April 18, 2024

The 1.4–1.8 μm eye-safe lasers have been widely used in the fields of laser medicine and laser detection and ranging. The diamond Raman lasers are capable of delivering excellent characteristics, such as good beam quality concomitantly with high output power. The intra-cavity diamond Raman lasers have the advantages of compactness and low Raman thresholds compared to the external-cavity Raman lasers. However, to date, the intra-cavity diamond cascaded Raman lasers in the spectral region of the eye-safe laser have an output power of only a few hundred milliwatts. A 1485 nm Nd:YVO_4/diamond intra-cavity cascaded Raman laser is reported in this paper. The mode matching and stability of the cavity were optimally designed by a V-shaped folded cavity, which yielded an average output power of up to 2.2 W at a pulse repetition frequency of 50 kHz with a diode to second-Stokes conversion efficiency of 8.1%. Meanwhile, the pulse width of the second-Stokes laser was drastically reduced from 60 ns of the fundamental laser to 1.1 ns, which resulted in a high peak power of 40 kW. The device also exhibited single longitudinal mode with a narrow spectral width of < 0.02 nm.

Keywords: diamond; intra-cavity; Raman lasers; eye-safe lasers; high peak-power.
DOI: 10.3788/COL202422.041402

1. Introduction

The 1.4–1.8 μm lasers combine the advantages of being eye-safe and high atmospheric transmittance, providing them with important applications in fields, such as laser medicine and laser detection and ranging (LIDAR)[1–3]. In order to achieve laser emissions in such a range, several methods have been exploited. For instance, Er^{3+} doped or Er^{3+}/Yb^{3+} co-doped fiber lasers can achieve continuous wave output of up to hundreds of watts[4–6]. However, the peak power and spectral linewidth of fiber lasers are generally limited because of the nonlinear effects of the fibers[7]. Another method is the Er^{3+} doped crystalline lasers, which are capable of providing high peak and average powers at 1.6 μm[8,9]. However, this usually requires pump sources with high brightness and narrow linewidths for efficient operation, thus inevitably increasing the complexity and cost of the system. In addition, the optical parametric oscillators (OPOs) are also an important and widely reported approach to realizing the eye-safe lasers. The commonly used OPO crystals to realize eye-safe laser emission include $KTiOAsO_4$(KTA), $KTiOPO_4$(KTP), and $RbTiOPO_4$(RTP). The OPOs have the advantage of pulse compression, which is beneficial for obtaining narrow pulse lasers. However, the phase matching requirements of OPO crystals, as well as thermal effects, are likely to cause problems such as system instability and poor beam quality[10–12].

Stimulated Raman scattering (SRS), which is a third-order nonlinear effect, has unique properties, such as automatic phase matching, pulse compression, being hole burning free, and Raman beam cleanup[13–16]. The crystalline Raman lasers are an efficient method of wavelength expansion and can deliver good beam quality concomitantly with high output power. Several Raman crystals have already been used to realize lasers with emission around 1.5 μm, such as $BaWO_4$, $BaTeMo_2O_9$, $GdVO_4$, and YVO_4[17–22]. Nevertheless, the output power is rather restricted, mainly because of the poor thermal conductivity generally faced by the above Raman crystals. Compared to conventional Raman crystals, a chemical vapor deposition (CVD) diamond has a high Raman gain coefficient (17 cm/GW @1 μm), a very wide transmission spectrum (> 0.23 μm), an

ultra-high thermal conductivity (2200 W/mK), and a large Raman shift (1332.3 cm^{-1}) and is well recognized as an outstanding Raman crystal[23–25]. Actually, for the past decade, diamond Raman lasers have experienced significant progress in characteristics, such as high-power, high-brightness, and various emission wavelengths[26–28].

Generally, there are two options for building diamond Raman lasers in the eye-safe band: one is to use the mature 1.06-μm laser ($^4F_{3/2} \rightarrow {}^4I_{11/2}$ Nd laser line) as the fundamental laser and to obtain the 1485 nm laser output by the second-Stokes shift, while the other is to use the 1.34 μm laser ($^4F_{3/2} \rightarrow {}^4I_{13/2}$ Nd laser line) as the fundamental laser and to obtain the 1634 nm laser output by the first-Stokes shift. Comparatively, although the latter requires only the first-Stokes shift, which could simplify the Raman conversion stage, the Nd^{3+} doped gain medium exhibits a larger emission cross section at 1.06 μm than at 1.34 μm, and the thermal effect is relatively weak because of the lower quantum defect at 1.06 μm and thus it is favorable for transferring the system thermal load more to the Raman crystal and for reducing the thermal effect of the Nd^{3+}-doped gain medium. Considering exceptionally high thermal conductivity of the diamond will be more beneficial to the stable operation of the system. Currently, the eye-safe diamond Raman lasers pumped by 1.06 μm fundamental lasers generally adopt external-cavity structures. It is well known that the structures of the intra-cavity have the advantages of compactness and low Raman thresholds compared to the structures of the external-cavity. However, due to the fact that more optical components are needed in the intra-cavity, the design of the cavity requires more comprehensive consideration of the thermal effect of the crystals, the cavity mode matching, and the cavity stability, which is therefore more difficult to realize and less reported so far. In 2010, Lubeigt *et al.* observed for the first time a second-Stokes emission (1485 nm) in an intra-cavity diamond Raman laser. The diamond sample used in the experiment had a high intracavity absorption loss of 2% at 1064 nm (round trip). This high loss as well as the unoptimized output coupler led to an average output power of only 30 mW[29]. In 2020, Yang *et al.* achieved an intra-cavity diamond Raman laser with a tunable output coupler by using a Brewster plate and investigated its effect on the performance of the Raman laser. Ultimately, a 1485 nm second-Stokes output power of about 0.12 W was obtained[30]. From this point of view, the output power, especially the peak power, which is critical for practical applications such as long-distance high-resolution measurements, of the eye-safe intra-cavity diamond Raman lasers is still in dire need of further improvement.

Here, we proposed a V-shaped folded cavity to achieve efficient operation of an eye-safe intra-cavity diamond cascaded Raman laser. On the one hand, the thermal effect of the laser crystal was mitigated due to the utilization of composite crystal and in-band pumping, and on the other hand, the mode matching and cavity stability are promoted by the V-shaped folded cavity. As a result, an average output power of 2.2 W with a diode to second-Stokes conversion efficiency of 8.1% has been successfully obtained. The pulse width of the second-Stokes laser was drastically reduced from 60 ns of the fundamental laser to 1.1 ns due to the Raman pulse compression, and this led to a peak power of up to 40 kW. Moreover, the device also exhibited a single longitudinal mode without an additional mode selection with a narrow spectral width of < 0.02 nm. The above results offer a new route for realizing high peak-power and narrow linewidth eye-safe intra-cavity diamond Raman lasers.

2. Experimental Setup

Figure 1 shows the schematic setup of the experimental system. A 65 W 880 nm fiber-coupled laser diode was used for in-band pumping. For the output coupling fiber, the numerical aperture of 0.22 and the core diameter of 200 μm were used. A 1:3 coupler was utilized for coupling the pump beam into an *a*-cut Nd:YVO_4 composite crystal, where the pump spot on the composite crystal had a diameter of about 600 μm. The dimension of the composite crystal was 4 mm × 4 mm × 20 mm, including a 16 mm length of Nd:YVO_4 with Nd^{3+} doping concentration of 0.3% in the middle and 2 mm length of pure YVO_4 at both ends. The composite crystal had an antireflection (AR) coating at the pump wavelength and the fundamental wavelength ($R < 0.2\%$). Our previous work has demonstrated that the composite crystals and the in-band pumping are effective in mitigating the thermal effect of the laser crystals[31]. An acousto-optic *Q*-switch (Gooch & Housego) with an operating wavelength of 1064 nm was used as the actively *Q*-switched element in the experiments. The Raman crystal was an uncoated CVD-diamond (2 mm × 2 mm × 7 mm), which was cut for beam to propagate in the ⟨110⟩ direction. The direction of the fundamental laser polarization was adjusted to match the direction of diamond ⟨111⟩, which maximizes the Raman gain[28]. Both the Nd:YVO_4 and the diamond were wrapped in indium foil and then placed in a copper block with water cooling at 18°C. The output power was measured by a power meter (PM100D) and a detector (S425C-L). The pulse characteristics were detected with an oscilloscope (DSO9254A, 2.5 GHz bandwidth, 98 ps rise time/fall time) and a photodetector (DET08CL/M, 5 GHz bandwidth, 70 ps rise time and 110 ps fall time). The laser spectra were recorded by an optical spectrum analyzer with a high wavelength resolution of 0.02 nm (Yokogawa, AQ6370C).

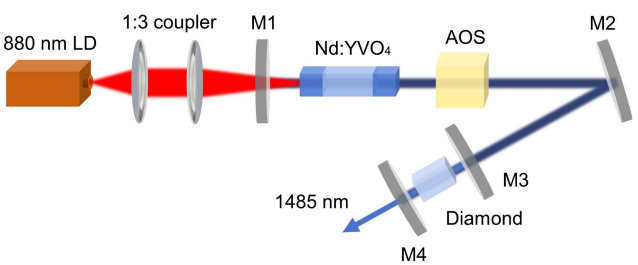

Fig. 1. Schematic setup of the V-shaped folded intra-cavity Nd:YVO_4/diamond eye-safe Raman laser. M1, input mirror; M2, folding mirror; M3, dichroic mirror; M4, output coupler; AOS, acousto-optic *Q*-switch.

The cavity was designed as a V-shaped folded cavity rather than a traditional straight cavity since it can provide better mode matching and ensure a small fundamental laser spot on the diamond. In fact, the V-shaped folded cavity has been widely proved to be an effective way for improving performance of the Raman lasers[32–35]. The flat input mirror M1 had a highly transmissive (HT) coating at 880 nm ($T > 95\%$) and a highly reflective (HR) coating at 1064 nm ($R > 99.8\%$). The plane-concave folding mirror M2 (radius of curvature of 100 mm) had the same coating as the M1. The flat output coupler M4 had an HR coating at 1064 nm and 1240 nm ($R > 99.8\%$) and an HT coating at 1485 nm ($T = 77.9\%$). Here, the fundamental cavity consisted of M1, M2, and M4. The total cavity length was 265 mm, where M1 and M2 were spaced 203 mm apart and M2 and M4 were spaced 62 mm apart. The M3 and M4 formed a Raman cavity, of which M3 was a plane dichroic mirror. The coating of M3 was designed to be HR at 1240 nm and 1485 nm ($R > 99.8\%$) and HT at 1064 nm ($T > 99\%$). The Raman cavity length was as short as 10 mm.

3. Results and Discussions

We first consider the mode matching under different thermal lens focal lengths by using the ABCD transfer-matrix theory. Figure 2(a) shows the calculated fundamental laser (1064 nm) beam radius distribution in the cavity under a thermal lens focal length of 300 mm. The fundamental laser on the Nd:YVO_4 has a beam size of 213 μm × 246 μm, which is slightly lower than the beam radius of the pump (300 μm), thus ensuring the efficient utilization of the pump beam. Due to the oblique incidence of the beam onto the folding mirror M2, the convergence points of the beam in the tangential plane (T) and sagittal plane (S) are misaligned, resulting in the astigmatism. The fundamental laser on the diamond has a beam size of 72 μm × 80 μm, which is significantly reduced compared to that in the straight cavity case (~120 μm in our experiments, not given). This will favor the enhancement of the fundamental laser power density on the diamond and thus the improvement of the Raman conversion efficiency.

Figure 2(b) shows the fundamental laser beam radius on both the Nd:YVO_4 and the diamond under different thermal lens focal lengths. In the case of a thermal lens with a focal length as small as 170 mm, the cavity is able to maintain a well-matched relationship between the pump and the fundamental laser. Correspondingly, the beam radius of the fundamental laser on the diamond can be well kept below 100 μm. The above results indicate that the V-shaped folded cavity in this work has a good thermal stability, which will ensure a high performance, especially a high output power in the following.

Next, we investigate the output characteristics of the fundamental laser. This was done by removing M3 and M4 and utilizing a flat mirror with 1064 nm partially transmissive (PT) coating ($T = 10\%$) as the output coupler. The power transfer characteristic for the fundamental laser at a pulse repetition frequency (PRF) of 50 kHz is shown in Fig. 3(a). The fundamental laser has a threshold of around 0.7 W. The output power is very stable and increases linearly with the increasing pump intensity. The average output power reaches 12.74 W without saturation when the incident pump power reaches 27.2 W, and the conversion efficiency is up to 46.8%. In order to prevent damage to the laser crystals and the cavity mirrors, we did not further increase the incident pump power during the experiments. The above results verify that the folded cavity is well designed and maintains good stability under such a high pump level. Figure 3(b) shows the fundamental laser emission spectrum, which gives a spectral width of 0.15 nm. A single pulse shape of the fundamental laser with a pulse width of 60 ns is shown in the inset of Fig. 3(b). Since the long cavity length tends to cause multiple longitudinal mode oscillations, it is likely that the multiple peaks of the fundamental laser pulse shape are caused by the beat frequency of multiple fundamental longitudinal modes[36].

Subsequently, we systematically investigate the output characteristics of the Nd:YVO_4/diamond second-Stokes Raman laser. The threshold of the second-Stokes laser is 3.95 W, as shown in Fig. 4(a). When the incident pump power gets to 27.2 W, the average output power and pulse energy reach 2.2 W and 44 μJ, respectively, and the corresponding conversion efficiency is up to 8.1%. This result is significantly better than that of the straight cavity (0.12 W in Ref. [30], and 0.5 W in our experiment, not given), which again validates the unique advantages of the folded cavity in mode matching and reduces the fundamental laser beam radius on the Raman crystals. In addition, the second-Stokes laser output power has not decreased over the entire incident pump power range[37,38], which further indicates that the thermal effects are well controlled.

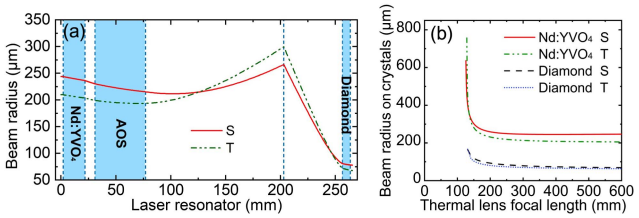

Fig. 2. (a) The fundamental laser beam radius distribution in the cavity. (b) The fundamental laser beam radius on both the Nd:YVO_4 and the diamond under different thermal lens focal lengths.

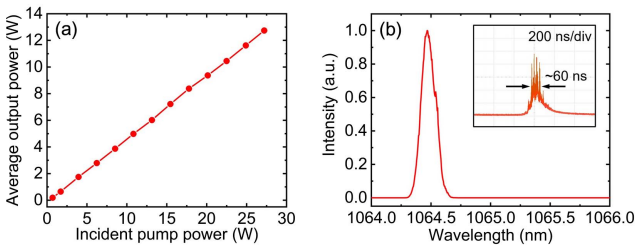

Fig. 3. (a) Power transfer characteristic for the fundamental laser at 50 kHz. (b) The fundamental laser emission spectrum at 27.2 W incident pump power. Inset: a single pulse shape.

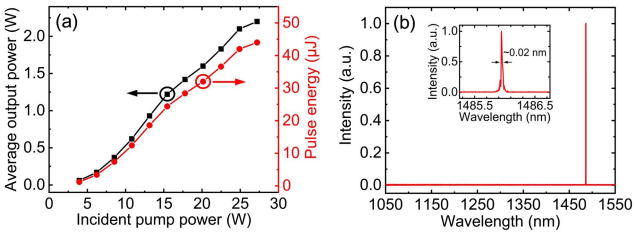

Fig. 4. Characteristics of the second-Stokes laser. (a) Average output power and pulse energy versus incident pump power at 50 kHz. (b) Emission spectrum for 27.2 W incident pump power. Inset: high-resolution spectrum.

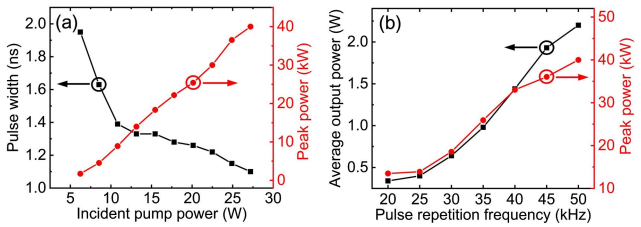

Fig. 5. Characteristics of the second-Stokes laser. (a) Pulse width and peak power versus incident pump power at 50 kHz. (b) Average output power and peak power versus different PRFs.

Figure 4(b) presents the second-Stokes emission spectrum for 27.2 W incident pump power. It can be seen that only the second-Stokes emission can be observed, while the fundamental and the first-Stokes emission can be hardly seen. This is mainly attributed to the efficient Raman conversion as well as the low transmission at the fundamental laser and the first-Stokes laser of the output coupler M4. According to the Raman laser theoretical model[39], in order to realize efficient second-Stokes lasers, the threshold of the second-Stokes laser is required to be sufficiently higher than that of the first-Stokes laser so that the robust first-Stokes field can be established, which effectively depletes the fundamental laser and increases the second-Stokes gain. The coating design of output coupler M4 realized efficient cascaded Raman conversion. In addition, the Raman conversion efficiency was also effectively improved by reducing the spot size of the fundamental laser on the diamond and adjusting the polarization direction of the fundamental laser to match the direction of diamond ⟨111⟩. The highly resolved spectrum of the second-Stokes emission is shown in the inset of Fig. 3(b), which shows a center wavelength located at 1485.9 nm and a resolution-limited linewidth of only 0.02 nm (2.72 GHz). Considering that the cavity length of the Stokes cavity is only 10 mm, which corresponds to a longitudinal mode spacing of about 7.5 GHz, we speculate that the second-Stokes laser is working in the single longitudinal mode. It should be mentioned that no additional longitudinal mode selector was used in this work. The single longitudinal mode can be obtained, probably due to the fact that the linewidth of the fundamental laser (0.15 nm, 39 GHz) is narrower than the Raman linewidth of the diamond (45 GHz). Therefore, considering the hole burning free characteristic of the SRS, in an ideal case, the single Stokes mode can effectively extract all longitudinal modes of the fundamental lasers[32,40]. Moreover, the Stokes cavity is also short enough to prevent multiple longitudinal mode oscillations. The observation of the single longitudinal mode is similar to that reported by Ma *et al.* in the 1.6-μm diamond Raman laser based on the first-Stokes emission. They also achieved the single longitudinal mode output by using a shorter Stokes cavity (9 mm) and controlling the fundamental laser linewidth to be less than the diamond Raman linewidth[41]. The detailed performance of the single longitudinal mode in our diamond Raman laser could be investigated by the Fabry–Perot interferometer[42], which would be done in future.

Figure 5(a) shows the pulse width and peak power of the second-Stokes laser as a function of the incident pump power at 50 kHz. The pulse width is less than 2 ns and it decreases with the increasing pump intensity. The pulse width could be as narrow as 1.1 ns at 27.2 W, which is significantly shortened compared to that of the fundamental laser and could be mainly attributed to the Raman pulse compression[15]. Additionally, the cascaded Raman process may also enhance the effect of the pulse compression[43]. In addition, such a short pulse width might also have arisen from the shorter Raman cavity, which will reduce the round trip time of the Stokes photons and make the build-up of the Stokes laser pulse faster. Correspondingly, the peak power of a single pulse reaches up to 40 kW. This is the highest peak power ever reported for the eye-safe diamond Raman lasers to the best of our knowledge. The average output power and peak power as a function of the PRF are shown in Fig. 5(b). As the PRF rises from 20 to 50 kHz, the average output power rises from 0.34 to 2.2 W, and the peak power rises from 13.49 to 40 kW. No obvious saturation or degradation has been observed, and we speculate that in addition to the well-designed V-shaped folded cavity, it could also be attributed to the short upper energy level lifetime of the Nd:YVO_4 crystal[44]. Limited by the *Q*-switch device, we were not able to employ a higher PRF in the experiment, and it is expected that the output power will continue to rise with the further rise of the PRF. Meanwhile, considering that Raman lasers with intra-cavity structures are extremely sensitive to losses in the intracavity[45], further improvement of the performance could be expected by using a diamond with AR coating in the future. In addition, compared to the common 880-nm laser diode used in our experiment, a wavelength-locked laser diode can be more favorable for improving the efficiency of the in-band pumping[46] and thus would be another effective way for improving the efficiency of the system.

Finally, it should be noted that the second-Stokes laser also exhibited a good beam quality and pulse stability at such a high peak-power. The beam quality (M^2) at the maximum output power was determined by a beam quality analyzer (Ophir, Nanoscan), and the M^2 was 1.33 and 1.76 for the horizontal and vertical direction, respectively. The slightly worsened M^2 from the near-diffraction-limited value and the inconsistency in both directions is caused by the astigmatism from the tilted placement of the folding mirror. Methods such as using a

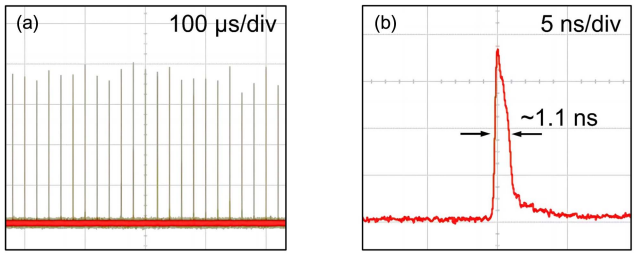

Fig. 6. Pulse characteristics of the second-Stokes laser at 27.2 W and 50 kHz. (a) Pulse train and (b) single pulse shape.

wedge-shaped laser crystal could be adopted to reduce the astigmatism. Figure 6(a) shows the pulse train of the second-Stokes laser at 27.2 W and 50 kHz. It can be observed that the intensity of the pulse train was relatively stable. The small intensity fluctuation could be aroused from the mechanical instability of the system. The single pulse shape [Fig. 6(b)] shows a pulse width of only 1.1 ns and a relatively smooth pulse profile.

4. Conclusion

In summary, we achieved a 1485 nm eye-safe intra-cavity diamond cascaded Raman laser with high peak power and narrow linewidth. Benefitting from the use of composite crystal and in-band pumping and the good mode matching provided by the V-shaped folded cavity, the device achieved an average output power of 2.2 W and a diode to second-Stokes conversion efficiency of 8.1%. The device also exhibited a high peak power of 40 kW and a single longitudinal mode with a spectral width of < 0.02 nm without any longitudinal mode selector. The above results offer a new route to realize high peak-power eye-safe intra-cavity diamond Raman lasers and pave the way towards applications such as high-resolution LIDAR over long ranges.

Acknowledgements

This work was financially supported by the Science and Technology Major Project of Henan Province (No. 221100230300) and the National Natural Science Foundation of China (No. 11774301).

References

1. S. H. Yun and S. J. J. Kwok, "Light in diagnosis, therapy and surgery," Nat. Biomed. Eng. **1**, 0008 (2017).
2. Y. X. Zhang, A. Carballo, H. T. Yang, *et al.*, "Perception and sensing for autonomous vehicles under adverse weather conditions: a survey," ISPRS J. Photogramm. Remote Sens. **196**, 146 (2023).
3. D. Wu, L. Yang, X. Chen, *et al.*, "Multi-channel pseudo-random coding single-photon ranging and imaging," Chin. Opt. Lett. **20**, 021202 (2022).
4. W. L. Yu, Q. R. Xiao, L. L. Wang, *et al.*, "219.6 W large-mode-area Er:Yb codoped fiber amplifier operating at 1600 nm pumped by 1018 nm fiber lasers," Opt. Lett. **46**, 2192 (2021).
5. W. Li, Q. Qiu, L. Yu, *et al.*, "Er/Yb co-doped 345-W all-fiber laser at 1535 nm using hybrid fiber," Opt. Lett. **48**, 3027 (2023).
6. H. Lin, Y. Feng, P. Barua, *et al.*, "405 W erbium-doped large-core fiber laser," in *Laser Congress 2017 (ASSL, LAC)* (2017), paper ATh4A.2.
7. I. Pavlov, E. Dulgergil, E. Ilbey, *et al.*, "Diffraction-limited, 10-W, 5-ns, 100-kHz, all-fiber laser at 1.55 μm," Opt. Lett. **39**, 2695 (2014).
8. S. Setzler, M. Shaw, M. Kukla, *et al.*, "A 400 W cryogenic Er:YAG laser at 1645 nm," Proc. SPIE **7686**, 76860C (2010).
9. L. Harris, M. Clark, P. Veitch, *et al.*, "Compact cavity-dumped Q-switched Er:YAG laser," Opt. Lett. **41**, 4309 (2016).
10. J. Meng, C. Li, Z. Cong, *et al.*, "Investigations on beam quality improvement of an NCPM-KTA-based high energy optical parametric oscillator using an unstable resonator with a Gaussian reflectivity mirror [Invited]," Chin. Opt. Lett. **20**, 091401 (2022).
11. Y. Duan, H. Zhu, Y. Ye, *et al.*, "Efficient RTP-based OPO intracavity pumped by an acousto-optic Q-switched Nd:YVO_4 laser," Opt. Lett. **39**, 1314 (2014).
12. H. Zhu, J. Guo, Y. Duan, *et al.*, "Efficient 1.7 μm light source based on KTA-OPO derived by Nd:YVO_4 self-Raman laser," Opt. Lett. **43**, 345 (2018).
13. R. Casula, J. P. Penttinen, M. Guina, *et al.*, "Cascaded crystalline Raman lasers for extended wavelength coverage: continuous-wave, third-Stokes operation," Optica **5**, 1406 (2018).
14. O. Lux, S. Sarang, O. Kitzler, *et al.*, "Intrinsically stable high-power single longitudinal mode laser using spatial hole burning free gain," Optica **3**, 876 (2016).
15. R. Frey, A. Demartino, and F. Pradere, "High-efficiency pulse compression with intracavity Raman oscillators," Opt. Lett. **8**, 437 (1983).
16. Y. Duan, Y. Sun, H. Zhu, *et al.*, "YVO_4 cascaded Raman laser for five-visible-wavelength switchable emission," Opt. Lett. **45**, 2564 (2020).
17. Z.-P. Wang, D.-W. Hu, X. Fang, *et al.*, "Eye-safe Raman laser at 1.5 μm based on $BaWO_4$ crystal," Chin. Phys. Lett. **25**, 122 (2008).
18. H. N. Zhang, P. Li, Q. P. Wang, *et al.*, "High-power dual-wavelength eye-safe ceramic Nd:YAG/$SrWO_4$ Raman laser operating at 1501 and 1526 nm," Appl. Opt. **53**, 7189 (2014).
19. S. D. Liu, J. J. Zhang, Z. L. Gao, *et al.*, "Generation of 1.3 μm and 1.5 μm high-energy Raman radiations in alpha-$BaTeMo_2O_9$ crystals," Opt. Mater. **36**, 760 (2014).
20. L. Fan, J. Shen, X. Y. Wang, *et al.*, "Efficient continuous-wave eye-safe Nd:YVO_4 self-Raman laser at 1.5 μm," Opt. Lett. **46**, 3183 (2021).
21. Y. F. Chen, "Efficient 1521-nm Nd:$GdVO_4$ Raman laser," Opt. Lett. **29**, 2632 (2004).
22. H. Chen, Q. Lou, J. Dong, *et al.*, "High-efficiency 1598.5-nm third Stokes Raman laser based on barium nitrate crystal," Chin. Opt. Lett. **4**, 404 (2006).
23. Q. Gong, M. Zhang, C. Lin, *et al.*, "Analysis of thermal effects in kilowatt high power diamond Raman lasers," Crystals **12**, 1824 (2022).
24. V. G. Savitski, S. Reilly, and A. J. Kemp, "Steady-state Raman gain in diamond as a function of pump wavelength," IEEE J. Quantum Electron. **49**, 218 (2013).
25. A. A. Kaminskii, V. G. Ralchenko, and V. I. Konov, "CVD-diamond–a novel $\chi^{(3)}$-nonlinear active crystalline material for SRS generation in very wide spectral range," Laser Phys. Lett. **3**, 171 (2006).
26. R. J. Williams, O. Kitzler, Z. X. Bai, *et al.*, "High power diamond Raman lasers," IEEE J. Sel. Top. Quantum Electron. **24**, 1602214 (2018).
27. S. Antipov, A. Sabella, R. J. Williams, *et al.*, "1.2 kW quasi-steady-state diamond Raman laser pumped by an $M^2 = 15$ beam," Opt. Lett. **44**, 2506 (2019).
28. D. T. Echarri, K. Chrysalidis, V. N. Fedosseev, *et al.*, "Broadly tunable linewidth-invariant Raman Stokes comb for selective resonance photoionization," Opt. Express **28**, 8589 (2020).
29. W. Lubeigt, G. M. Bonner, J. E. Hastie, *et al.*, "An intra-cavity Raman laser using synthetic single-crystal diamond," Opt. Express **18**, 16765 (2010).
30. H. L. Yang, Y. Chen, K. L. Ding, *et al.*, "Investigation of a highly compact intracavity actively Q-switched cascade diamond Raman laser," Appl. Opt. **59**, 9715 (2020).
31. L. Fan, X. Wang, X. Zhao, *et al.*, "First-Stokes and second-Stokes multi-wavelength continuous-wave operation in Nd:YVO_4/$BaWO_4$ Raman laser under in-band pumping," Chin. Opt. Lett. **18**, 111401 (2020).
32. Q. Sheng, R. Li, A. J. Lee, *et al.*, "A single-frequency intracavity Raman laser," Opt. Express **27**, 8540 (2019).
33. H. J. Ma, X. Wei, S. B. Dai, *et al.*, "Intra-cavity diamond Raman laser at 1634 nm," Opt. Express **29**, 31156 (2021).
34. S. W. Peng, X. X. Huang, and S. H. Ding, "Folded-resonator LD side-pumped acousto-optically Q-switched Nd:YAG/$SrWO_4$ solid-state Raman laser," Infrared Phys. Technol. **127**, 104368 (2022).

35. H. H. Chen, W. J. Hu, X. Wei, *et al.*, "High beam quality yellow laser at 588 nm by an intracavity frequency-doubled composite Nd:YVO_4 Raman laser," Opt. Express **31**, 8494 (2023).
36. J. M. Jelínek, O. Kitzler, H. Jelínková, *et al.*, "CVD-diamond external cavity nanosecond Raman laser operating at 1.63 μm pumped by 1.34 μm Nd:YAP laser," Laser Phys. Lett. **9**, 35 (2012).
37. H. Zhu, Y. Duan, G. Zhang, *et al.*, "Yellow-light generation of 5.7 W by intracavity doubling self-Raman laser of YVO_4/Nd:YVO_4 composite," Opt. Lett. **34**, 2763 (2009).
38. J. Guo, H. Zhu, S. Chen, *et al.*, "Yellow, lime and green emission selectable by BBO angle tuning in *Q*-switched Nd:YVO_4 self-Raman laser," Laser Phys. Lett. **15**, 075803 (2018).
39. R. J. Williams, D. J. Spence, O. Lux, *et al.*, "High-power continuous-wave Raman frequency conversion from 1.06 μm to 1.49 μm in diamond," Opt. Express **25**, 749 (2017).
40. E. Granados, C. Granados, R. Ahmed, *et al.*, "Spectra synthesis of multimode lasers to the Fourier limit in integrated Fabry-Perot diamond resonators," Optica **9**, 317 (2022).
41. H. J. Ma, X. Wei, H. Zhao, *et al.*, "Nanosecond pulsed single longitudinal mode diamond Raman laser in the 1.6 μm spectral region," Opt. Lett. **47**, 2210 (2022).
42. N. Ismail, C. C. Kores, D. Geskus, *et al.*, "Fabry-Pérot resonator: spectral line shapes, generic and related Airy distributions, linewidths, finesses, and performance at low or frequency-dependent reflectivity," Opt. Express **24**, 16366 (2016).
43. J. Liu, X. Ding, P. Jiang, *et al.*, "High-performance second-Stokes generation of a Nd:YVO_4/YVO_4 Raman laser based on a folded coupled cavity," Opt. Express **26**, 10171 (2018).
44. P. B. Jiang, J. S. Ni, H. W. Zhang, *et al.*, "High-power and high-energy Nd:YAG-Nd:YVO_4 hybrid gain Raman yellow laser," Opt. Express **28**, 24088 (2020).
45. J. A. Piper and H. M. Pask, "Crystalline Raman lasers," IEEE J. Sel. Top. Quantum Electron. **13**, 692 (2007).
46. Q. Sheng, X. Ding, B. Li, *et al.*, "Efficient Nd:YVO_4 self-Raman laser in-band pumped by wavelength-locked laser diode at 878.7 nm," J. Opt. **16**, 105206 (2014).